RSC Advances

PAPER

View Article Online
View Journal | View Issue

Cite this: *RSC Adv.*, 2025, **15**, 26

Molecular interactions between surface-active ionic liquids based on 2-hydroxyethylammonium laurate with gabapentin: electrical conductivity and surface tension studies†

Mohammad Bagheri, Fariba Ghaffari, Hemayat Shekaari, * Masumeh Mokhtarpour and Behrang Golmohammadi

Surface active ionic liquids (SAILs), offer potential advantages for pharmaceutical applications. Given the low permeability of gabapentin, an antiepileptic drug, in the gastrointestinal tract as classified by the Biopharmaceutics Classification Systems (BCS), understanding the micellization behavior of SAILs is essential for developing effective drug delivery systems to improve gabapentin bioavailability. This study explores the micellization and thermophysical behavior of SAILs (2-hydroxyethyl)ammonium laurate [2-HEA][Lau], bis(2-hydroxyethyl)ammonium laurate [BHEA][Lau], and tris(2-hydroxyethyl)ammonium laurate [THEA][Lau] in the presence of aqueous gabapentin solution at varied temperatures through COSMO analysis, electrical conductivity and surface tension measurements. The electrical conductivity and surface tension measurements were employed to obtain the critical micelle concentration (CMC) and related thermophysical properties of binary (SAILs + water) and ternary (SAILs + water + gabapentin) systems at (298.15 to 318.15) K such as Π (interface surface pressure), σ_{CMC} (CMC point surface tension), A_{min} (minimum surface area occupied per molecule), Γ_{max} (Gibbs maximum excess surface concentration) have been computed. For better understanding the interactions between these components, Conductor like Screening Model (COSMO) was utilized. The study revealed that CMC values increased with temperature but decreased with increasing gabapentin concentration. Finally, interactions between SAILs and gabapentin were investigated through limiting molar conductivity Λ_0, and association constant K_A, determination.

Received 15th September 2024
Accepted 5th November 2024

DOI: 10.1039/d4ra06670g

rsc.li/rsc-advances

1. Introduction

Surface-active ionic liquids (SAILs) are a promising class of molecules that combine the desirable properties of surfactants and ionic liquids (ILs). They possess both amphiphilic characteristics, allowing them to interact with both water and oil, and the tunability of ILs. This unique combination makes SAILs ideal candidates for enhancing the solubility and permeability of drugs in pharmaceutical applications and various industrial processes.[1–3] The utilization of SAILs has been shown to increase the bioavailability and efficacy of drugs, thus reducing the required dosage and potential side effects associated with higher drug concentrations. Incorporating SAILs in drug processing offers a promising approach to optimizing drug efficiency, minimizing drug consumption, and improving therapeutic outcomes for patients. Epilepsy affects an estimated 50 million people globally, solidifying its position as one of the most prevalent neurological disorders. This translates to a staggering prevalence of approximately 1 in 120 individuals worldwide living with epilepsy.[4,5]

Gabapentin, an anticonvulsant drug, is one of the commonly prescribed medications for the treatment of epilepsy. Gabapentin's therapeutic potential is accompanied by a range of side effects. Common occurrences include drowsiness and impaired coordination. Additionally, the medication may manifest more severe side effects, such as mood alterations or allergic reactions.[6,7] Incorporating SAILs in drug delivery systems holds significant potential to optimize the efficiency of drug delivery, including enhancing the permeability of drugs like gabapentin. Ethanolamine based ionic liquids (2-hydroxyethylammonium based IL) got considerable attention due to nontoxicity and biocompatibility for pharmaceutical and clinical uses. Lauric acid, also known as dodecanoic acid ($C_{12}H_{24}O_2$), is a medium-chain saturated fatty acid (MCSFA) that is predominantly found in coconut oil.[8] These carboxylic acids recently have been used in neutralization reaction with ethanolamine that led to production of protic, easy preparable and cost-effective SAILs

Department of Physical Chemistry, University of Tabriz, Tabriz, Iran. E-mail: hemayatt@yahoo.com; Fax: +984133340191; Tel: +984133393094

† Electronic supplementary information (ESI) available. See DOI: https://doi.org/10.1039/d4ra06670g

such as (2-hydroxyethyl)ammonium laurate ([2-HEA][Lau]), bis(2-hydroxyethyl)ammonium laurate ([BHEA][Lau]), and tris(2-hydroxyethyl)ammonium laurate ([THEA][Lau]).

The surface activity characteristics exhibited by the investigated SAILs, have led to the determination of their critical micelle concentration (CMC), a crucial criterion for monitoring their behavior in aqueous solutions. The formation of CMC in the aqueous media could be used as a emulsifier of the aqueous media and as agent to improve drug adsorption and penetration through cell membrane. Several approaches can be employed to study CMC, each offering unique insights.[9,10] Among the various techniques available, electrical conductivity and static surface tension measurement using the Wilhelmy plate method stand out as highly accurate and efficient methods for determining CMC.[11–13] These established methods provide reliable data for researchers investigating surfactant behavior and CMC phenomena. Electrical conductivity titration was employed to determine the CMC of [2-HEA][Lau], [BHEA][Lau], and [THEA][Lau] in aqueous media.

In this work, the impact of gabapentin on CMC was investigated using the electrical conductivity and surface tension method at varying drug gabapentin concentrations. Subsequently, the thermodynamic properties of CMC, including Gibbs free energy of micellization, were calculated. The obtained data facilitated the calculation of various thermodynamic properties, such as excess surface energy and Gibbs free energy of micellization. In this study, COSMO calculations were carried out to gain insights into the thermophysical, thermodynamic, and micellar properties of these systems. From COSMO calculations, we were able to obtain various parameters such as sigma profile, surface area of cavity, total volume of cavities, and dielectric solvation energies.

2. Materials and methods

2.1. Chemicals

The specification about the utilized chemicals including their chemical name, chemical formula, provenance, molar mass, purity, and chemical structure have been tabulated within the Table 1.

2.2. Synthesis of ethanolamine-based SAILs

The SAILs can be easily synthesized by neutralization reaction of mono, di, and triethanolamines with lauric acid. The reaction led to formation of SAILs (2-hydroxyethyl)ammonium laurate ([2-HEA][Lau]), bis(2-hydroxyethyl)ammonium laurate ([BHEA][Lau]), and

Table 1 Descriptions of the used chemicals

Chemical name	Chemical formula	Provenance	Molar mass (g mol^{-1})	Mass fraction (purity)	Structure
Gabapentin	$C_9H_{17}NO_2$	Merck	171.24	99%	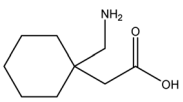
Monoethanolamine (2-hydroxyethylammine)	C_2H_7NO	Merck	61.084	99%	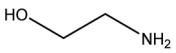
Diethanolamine (bis-2-hydroxyethylammine)	$C_4H_{11}NO_2$	Merck	105.14	99%	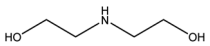
Triethanolamine (tris-2-hydroxyethylammine)	$C_6H_{15}NO_3$	Merck	149.188	99%	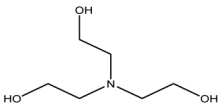
Lauric acid	$C_{12}H_{24}O_2$	Merck	200.320	99%	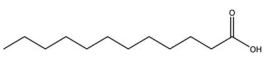
(2-Hydroxyethylammonium laurate) [2-HEA]Lau	$C_{14}H_{31}NO_3$	Synthesized	261.41	>98%	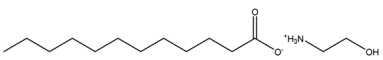
Bis-(2-hydroxyethylammonium laurate) [BHEA]Lau	$C_{16}H_{35}NO_4$	Synthesized	305.46	>98%	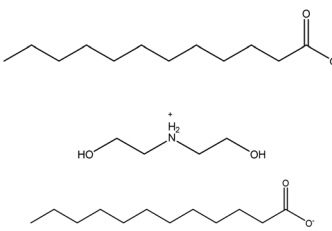
Tris-(2-hydroxyethylammonium laurate) [THEA]Lau	$C_{18}H_{39}NO_5$	Synthesized	349.51	>98%	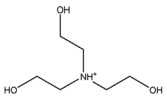

tris(2-hydroxyethyl)ammonium laurate ([THEA][Lau]). A dropping funnel was used to add equimolar amount of lauric acid into the flask containing ethanolamines and stirred vigorously. After finalizing the addition of the acid, the mixture has been stirred for 24 hours at room temperature to complete the reaction. Through the characterization of synthesized SAILs by ^{1}H-NMR and IR spectra (provided in ESI material in Fig. S1–S6† along with their appropriate interpretation), approximate high yield of 98% was achieved.[14] A comprehensive analysis of IR spectra (Fig. S1–S3†) provides invaluable insights into the molecular structure and composition of the synthesized SAILs. Characteristic absorption peaks at 566 and 719 cm^{-1} confirm the presence of the COO^- functional group, a key indicator of the compounds' surface-active properties. Additionally, the strong peaks at 2849 and 2920 cm^{-1} are indicative of the antisymmetric and symmetric stretching vibrations of CH_2 groups, respectively, suggesting the presence of a long alkyl chain. The C=O stretching vibration at 1709 cm^{-1} is indicative of carboxylic acid carbonyls. Furthermore, the antisymmetric stretching vibrations of CH_3; groups are observed at 1094 cm^{-1} as two weak peaks. The in-plane bending (914 cm^{-1}), symmetric (1468 cm^{-1}), and out-of-plane bending (1253 cm^{-1}) vibrations of the fatty acid carboxyl (COOH) groups are also observed in the spectra. In summary, the IR spectra analysis reveals the presence of the expected functional groups and vibrational modes associated with the molecular structure of the synthesized SAILs, confirming their overall composition and structural characteristics.[15] Notably, the presence of a peak around 3357 cm^{-1} in the spectra indicates the existence of an N–H bond, a strong bond commonly observed in SAILs.[16]

2.3. Instrumentation

2.3.1. Surface tension measurement. Surface tension measurements of aqueous solutions of SAILs were performed in the presence and absence of varying concentrations of gabapentin drug at a constant temperature of 298.15 K. A KRÜSS Easy Dyne K20 tensiometer (Germany) employing the Wilhelmy plate (PL22) method was utilized for measuring the surface tension of the studied systems. The accuracy of the instrument for measuring surface tension has been estimated to be in the range of ± 0.01 mN m^{-1}. The proper cleaning of the Wilhelmy plate between each measurement is necessary to obtain accurate data, the cleansing process is as follows at first, the plate was firstly rinsed with ultrapure, double distilled, deionized water, then by high-purity acetone (the specification of the material used has been provided in Table 1), and in the end the plate was heated to a red-hot state. The CMC of SAILs was determined by extrapolating the inflection point observed in the surface tension *versus* molality plot.

2.3.2. Electrical conductivity measurement, to maintain consistent and logical hierarchical organization within the document. A digital electrical conductivity meter (Metrohm model 712, Switzerland) and a dipping conductivity cell with platinized electrodes (with 0.867 cm^{-1} cell constant) were used to measure electrical conductivity. Aqueous KCl solution with 0.01 mol kg^{-1} molality was used to calibrate and calculate the cell constant. The conductivity electrode cell was inserted into the precisely measured mass of doubly distilled, deionized, and degassed water, and was tightly sealed. Using a syringe, the defined, weighed SAIL was injected into the water solution-filled sample holder and continuously stirred. To maintain the temperature with a precision of 0.02 K, water from a thermostatically controlled bath (Julabo ED Germany) was circulated around the double-walled sample holder to maintain the temperature. The uncertainty in the measured specific conductivity was estimated to be less than 0.5 percent.

3. Results and discussion

3.1. Critical micelle concentration (CMC)

SAILs are amphiphilic molecules that show a tendency to form self-assembly or colloidal like structures in the solution phase above a particular concentration, which is termed as the CMC of the corresponding molecule. Above CMC, the aggregated SAILs exhibit special properties, which are not, in general, observed in the case of monomeric species.[17,18] Thus, in the current study, the most simple, reliable, accurate and commonly utilized techniques known as surface tension (presented in Tables 2 and S1†) and electrical conductivity (presented in Tables S2–S5†) were utilized in finding the CMC values of the studied SAILs ([2-HEA][Lau], [BHEA][Lau] and [THEA][Lau]). Then, the effect of gabapentin as a co-solute in CMC point was investigated. The measured electrical conductivity of SAILs in water were investigated at a temperature range (288.15 to 318.15) K, Also the related temperature utilized for measuring the surface tension of SAILs in water and aqueous gabapentin solution was 298.15 K.

The behavior of SAILs was studied through electrical conductivity and surface tension measurement, in electrical conductivity measurement, SAILs were undergone a complete ionization in solution, and so their specific conductivities, κ were found to increase gradually, by increasing the concentration of SAILs. However, after the addition of a certain amount of SAIL, the rising trending slope of the κ tends to show a moderated decrease. Thus, a sudden breakpoint was obtained in the plot of κ *versus* the concentration of aqueous gabapentin solution. The values of κ, for the studied systems have been listed in Tables S2–S5.† Also, a typical curve of such a plot has been presented in Fig. 1. In surface tension measurement, SAILs tend to aggregate on the surface of the solution upon addition due to their amphiphilic nature, which changes the surface properties of the solution (lowering the surface tension) by saturating the surface of the solution, after which, the next added SAILs into the solution causes the aggregated SAILs to penetrate the surface and inter the bulk phase of the solution and aggregate in numbers, ultimately form micelle like structures in the solution, the concentration which in that SAILs saturate and penetrate the surface and form colloidal like (micelle) structures in the solution are known as CMC. As illustrated in Fig. 2 and Table S1,† the measured surface tension, showed a decrement as the concentration of SAILs increased upon addition into the water and aqueous gabapentin solution, which is result of the fast saturation of the surface by high number of SAILs.

Table 2 Surface active parameters of SAILs in various aqueous gabapentin solutions[a] (from 0.0000 to 0.0500 mol kg^{-1}) at 298.15 K

CMC (mol m^{-3})	σ_{CMC} (mN m^{-1})	Π_{CMC} (mN m^{-1})	$10^3 \times \Gamma_{max}$(mol m^{-2})	A_{min} (Å^2)	ΔG_{mic} (kJ mol^{-1})	ΔG^0_{ad} (kJ mol^{-1})	G^s_{min} (kJ mol^{-1})
[2-HEA][Lau] + water							
1.3198	50.7	3.3	0.551	0.301	−31.068	−25.080	9.200
		2.3	0.177	0.941	−28.797	−15.768	28.720
		0.8	0.552	0.301	−27.079	−25.628	9.192
		−2.7	1.265	0.131	−24.909	−27.042	4.007
		−7.2	1.697	0.098	−23.406	−27.649	2.988
		−11	1.892	0.088	−22.478	−28.292	2.680
		−13.3	1.989	0.083	−21.833	−28.520	2.549
		−15.5	2.045	0.081	−21.298	−28.876	2.479
		−17.1	2.075	0.08	−20.879	−29.120	2.443
		−18.6	2.093	0.079	−20.434	−29.320	2.422
		−20	2.098	0.079	−20.161	−29.694	2.417
		−21.7	2.098	0.079	−19.847	−30.188	2.416
[2-HEA][Lau] in 0.0099 mol kg^{-1}concentration of aqueous gabapentin solution							
1.0503	48.3	1.69	0.736	0.226	−18.321	−16.023	6.636
		0.69	0.027	6.176	−16.368	9.293	181.525
		−0.81	0.76	0.219	−13.69	−14.756	6.425
		−4.31	1.411	0.118	−12.178	−15.233	3.46
		−9.31	1.919	0.087	−10.691	−15.542	2.543
		−12.71	2.092	0.079	−9.815	−15.891	2.333
		−16.01	2.144	0.077	−9.089	−16.556	2.277
		−18.11	2.128	0.078	−8.603	−17.113	2.294
		−19.81	2.088	0.08	−8.241	−17.726	2.337
		−21.41	2.021	0.082	−7.859	−18.455	2.416
		−22.71	1.941	0.086	−7.533	−19.233	2.515
		−23.61	1.872	0.089	−7.299	−19.913	2.608
[2-HEA][Lau] in 0.0301 mol kg^{-1}concentration of aqueous gabapentin solution							
0.8546	44.3	2.514	−0.342	−0.485	−18.321	−25.667	−12.941
		1.414	0.475	0.35	−15.52	−12.542	9.327
		−0.286	0.702	0.236	−14.102	−14.509	6.306
		−4.486	1.435	0.116	−11.981	−15.107	3.085
		−9.086	1.989	0.083	−10.747	−15.316	2.227
		−12.786	2.3	0.072	−9.854	−15.414	1.926
		−16.086	2.392	0.069	−9.176	−15.9	1.851
		−18.686	2.311	0.072	−8.603	−16.689	1.916
		−20.686	2.145	0.077	−8.221	−17.865	2.065
		−22.486	1.841	0.09	−7.81	−20.024	2.406
		−23.486	1.515	0.11	−7.504	−23.011	2.924
		−24.086	1.164	0.143	−7.248	−27.935	3.804
[2-HEA][Lau] in 0.0503 mol kg^{-1}concentration of aqueous gabapentin solution							
0.7833	40.4	1.824	−0.13	−1.278	−18.085	−32.118	−31.14
		0.724	0.480	0.346	−15.15	−13.642	8.429
		−1.976	1.097	0.151	−13.177	−14.978	3.689
		−5.176	1.497	0.111	−12.178	−15.635	2.703
		−9.976	2.064	0.08	−10.747	−15.581	1.961
		−14.176	2.328	0.071	−9.815	−15.905	1.739
		−17.676	2.405	0.069	−9.089	−16.441	1.683
		−19.776	2.37	0.070	−8.650	−16.995	1.708
		−22.276	2.245	0.074	−8.182	−18.104	1.803
		−23.676	2.096	0.079	−7.859	−19.155	1.931
		−25.076	1.873	0.089	−7.518	−20.909	2.161
		−25.976	1.628	0.102	−7.235	−23.187	2.486
[BHEA][Lau] in water							
1.0955	47.8	2.243	1.062	0.156	−18.724	−16.612	4.506
		1.143	0.041	4.038	−15.365	12.427	116.365
		−0.557	0.813	0.204	−13.507	−14.192	5.889
		−4.257	1.687	0.098	−11.799	−14.322	2.836
		−9.057	2.134	0.078	−10.747	−14.991	2.242
		−13.357	2.406	0.069	−9.777	−15.33	1.989

Table 2 (*Contd.*)

CMC (mol m^{-3})	σ_{CMC} (mN m^{-1})	Π_{CMC} (mN m^{-1})	$10^3 \times \Gamma_{max}$(mol m^{-2})	A_{min} (Å^2)	ΔG_{mic} (kJ mol^{-1})	ΔG^0_{ad} (kJ mol^{-1})	G^s_{min} (kJ mol^{-1})
		−16.457	2.486	0.067	−9.118	−15.737	1.925
		−19.157	2.48	0.067	−8.603	−16.327	1.929
		−21.257	2.429	0.068	−8.201	−16.953	1.97
		−23.057	2.346	0.071	−7.843	−17.672	2.04
		−24.557	2.239	0.074	−7.518	−18.488	2.138
		−25.757	2.136	0.078	−7.273	−19.33	2.24
[BHEA]Lau in 0.0100 mol kg^{-1}concentration of aqueous gabapentin solution							
0.9866	44.7	2.738	0.681	0.244	−17.975	−13.951	6.578
		1.638	0.134	1.236	−16.258	−4.067	33.315
		0.038	0.767	0.216	−13.887	−13.838	5.836
		−4.562	1.632	0.102	−12.078	−14.874	2.744
		−9.262	2.142	0.078	−10.805	−15.128	2.09
		−13.562	2.366	0.07	−9.854	−15.587	1.892
		−17.262	2.404	0.069	−9.118	−16.299	1.862
		−19.962	2.345	0.071	−8.603	−17.117	1.909
		−21.762	2.243	0.074	−8.201	−17.904	1.996
		−23.262	2.106	0.079	−7.843	−18.886	2.125
		−24.762	1.935	0.086	−7.504	−20.3	2.313
		−25.762	1.785	0.093	−7.26	−21.694	2.508
[BHEA][Lau] in 0.0303 mol kg^{-1}concentration of aqueous gabapentin solution							
0.8696	41.4	2.571	−0.041	−4.074	−18.582	−81.664	−101.65
		1.371	0.389	0.427	−15.816	−12.294	10.644
		−0.129	0.66	0.252	−14.388	−14.583	6.278
		−4.929	1.526	0.109	−12.078	−15.308	2.715
		−10.229	2.108	0.079	−10.691	−15.544	1.966
		−14.229	2.339	0.071	−9.777	−15.861	1.771
		−17.329	2.346	0.071	−9.147	−16.533	1.766
		−19.929	2.194	0.076	−8.58	−17.664	1.888
		−21.829	1.956	0.085	−8.163	−19.321	2.118
		−23.029	1.686	0.098	−7.843	−21.499	2.457
		−23.929	1.359	0.122	−7.547	−25.151	3.048
		−24.629	0.98	0.169	−7.273	−32.403	4.227
[BHEA][Lau] in 0.0498 mol kg^{-1}concentration of aqueous gabapentin solution							
0.8324	37.4	1.778	0.57	0.291	−18.582	−15.464	6.562
		0.678	0.094	1.767	−16.258	−9.042	39.83
		−1.022	0.86	0.193	−13.69	−14.878	4.352
		−5.422	1.626	0.102	−12.178	−15.512	2.301
		−11.122	2.312	0.072	−10.636	−15.447	1.619
		−15.122	2.51	0.066	−9.815	−15.84	1.491
		−18.922	2.521	0.066	−9.118	−16.623	1.484
		−21.422	2.407	0.069	−8.603	−17.503	1.555
		−23.922	2.208	0.075	−8.163	−18.999	1.695
		−25.022	1.994	0.083	−7.843	−20.389	1.876
		−26.222	1.712	0.097	−7.518	−22.831	2.185
		−27.122	1.436	0.116	−7.26	−26.15	2.606
[THEA][Lau] in water							
1.0063	44.2	2.269	0.666	0.249	−31.781	−28.376	6.639
		1.269	0.179	0.93	−28.606	−21.498	24.775
		−0.631	0.863	0.192	−26.627	−27.358	5.124
		−4.731	1.528	0.109	−24.909	−28.005	2.895
		−9.631	1.972	0.084	−23.642	−28.527	2.243
		−13.831	2.359	0.07	−22.478	−28.341	1.875
		−17.531	2.596	0.064	−21.804	−28.556	1.704
		−20.631	2.803	0.059	−21.274	−28.634	1.578
		−23.531	2.996	0.055	−20.838	−28.693	1.476
		−24.831	3.181	0.052	−20.468	−28.274	1.391
		−27.431	3.361	0.049	−20.145	−28.306	1.316
		−28.931	3.495	0.048	−19.929	−28.207	1.266

Table 2 (*Contd.*)

CMC (mol m^{-3})	σ_{CMC} (mN m^{-1})	Π_{CMC} (mN m^{-1})	$10^3 \times \Gamma_{max}$(mol m^{-2})	A_{min} (Å^2)	ΔG_{mic} (kJ mol^{-1})	ΔG^0_{ad} (kJ mol^{-1})	G^s_{min} (kJ mol^{-1})
[THEA][Lau] in 0.0101 mol kg^{-1}concentration of aqueous gabapentin solution							
0.8939	40.185	3.415	−0.412	−0.403	−18.321	−26.613	−9.757
		2.215	0.647	0.257	−16.052	−12.629	6.21
		−0.185	1.023	0.162	−14.338	−14.518	3.927
		−6.685	1.682	0.099	−12.178	−16.152	2.389
		−11.085	2.149	0.077	−10.924	−16.081	1.87
		−16.185	2.469	0.067	−9.777	−16.331	1.627
		−19.885	2.519	0.066	−9.118	−17.011	1.595
		−22.685	2.445	0.068	−8.603	−17.883	1.644
		−24.885	2.284	0.073	−8.182	−19.079	1.76
		−26.285	2.061	0.081	−7.826	−20.582	1.95
		−27.385	1.792	0.093	−7.518	−22.801	2.243
		−28.185	1.567	0.106	−7.312	−25.297	2.564
[THEA][Lau] in 0.0299 mol kg^{-1}concentration of aqueous gabapentin solution							
0.8324	39	2.3	0.473	0.351	−18.321	−13.454	8.252
		1.2	0.234	0.708	−16.052	−10.933	16.638
		−0.5	0.705	0.236	−14.338	−15.047	5.536
		−5.0	1.636	0.101	−12.283	−15.339	2.383
		−11.4	2.26	0.073	−10.691	−15.734	1.725
		−15.6	2.411	0.069	−9.854	−16.324	1.617
		−19.0	2.382	0.07	−9.176	−17.152	1.637
		−21.5	2.219	0.075	−8.603	−18.294	1.758
		−23.2	1.999	0.083	−8.182	−19.789	1.951
		−24.8	1.723	0.096	−7.81	−22.205	2.264
		−25.8	1.462	0.114	−7.533	−25.183	2.668
		−26.6	1.138	0.146	−7.248	−30.623	3.427
[THEA][Lau] in 0.0503 mol kg^{-1}concentration of aqueous gabapentin solution							
0.7150	33.9	2.111	−0.057	−2.931	−17.975	−55.237	−59.819
		0.911	0.458	0.363	−16.052	−14.061	7.407
		−0.689	0.661	0.251	−14.338	−15.38	5.129
		−5.489	1.553	0.107	−12.178	−15.713	2.182
		−11.589	2.466	0.067	−10.691	−15.391	1.374
		−16.389	2.927	0.057	−9.666	−15.265	1.158
		−20.289	2.997	0.055	−9.236	−16.006	1.131
		−23.389	2.874	0.058	−8.58	−16.718	1.179
		−25.589	2.666	0.062	−8.241	−17.837	1.271
		−27.689	2.305	0.072	−7.876	−19.887	1.47
		−29.089	1.883	0.088	−7.577	−23.026	1.8
		−29.889	1.156	0.144	−7.197	−33.044	2.931

[a] The standard uncertainties for molality, temperature and pressure were $u(C) = 0.001$ mol m^{-3}, $u(T) = 0.5$ K, and $u(P) = 0.01$ MPa respectively with level of confidence 0.95. The standard combined uncertainty for surface tension were about, $uc(\sigma) = 0.01$ mN m^{-1} (level of confidence 0.68), respectively.

SAILs with hydroxyethyl groups exhibit a hydrophilic head and a hydrophobic tail in aqueous solutions. As concentration increases, these molecules self-assemble into micelles above a critical micelle concentration (CMC). The structure of SAILs influences their CMC, with longer alkyl chains and more hydroxyethyl groups generally leading to lower CMC values. In the studied gabapentin solutions, SAILs demonstrated lower CMCs compared to water molecules, as evidenced by their faster surface saturation. The CMC values for these systems decreased with increasing temperature up to 313.15 K but then increased at higher temperatures.[17–20]

The variation of the electrical conductivity and the surface tension with the concentration of the studied SAILs have been observed to decrease with an increase in the concentration of gabapentin in the aqueous solution. This decrease in the CMC of SAILs can be attributed to the accumulation of gabapentin molecules in the solution, which disrupts the favorable interactions of water with the hydrophilic head groups of SAILs, as previously reported for interactions between surfactants and other additives.[21–24] This accumulation effect creates a less favorable environment for the hydrophobic tails of SAILs to reside in the bulk aqueous phase. To minimize this unfavorable interaction, the SAIL molecules preferentially aggregate with each other in the bulk phase of the aqueous gabapentin solution faster than water, which reduces the free SAIL molecules available in the solution, effectively lowering the overall CMC.

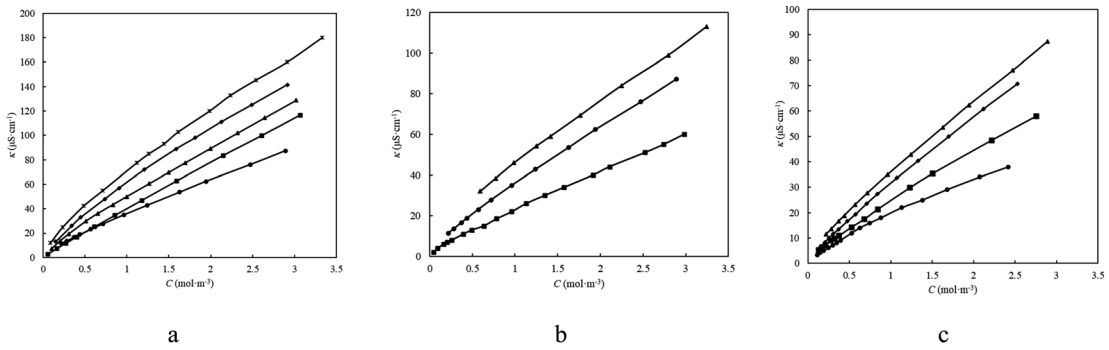

Fig. 1 Specific conductivity (κ) of, (a) [BHEA][Lau] in aqueous solutions at; ● 298.15 K, ■ 303.15 K,◆ 308.15 K, ▲ 313.15 K, * at 318.15 K, temperatures. (b) SAILs in aqueous solutions at 298.15 K; ▲ [2-HEA][Lau], ● [BHEA][Lau], ■ [THEA][Lau]. (c) [BHEA][Lau] in aqueous gabapentin solutions with different molality concentration of gabapentin (mol kg^{-1}); ▲, 0.0000, ◆, 0.0100, ■, 0.0300, ● 0.0500 at 298.15 K.

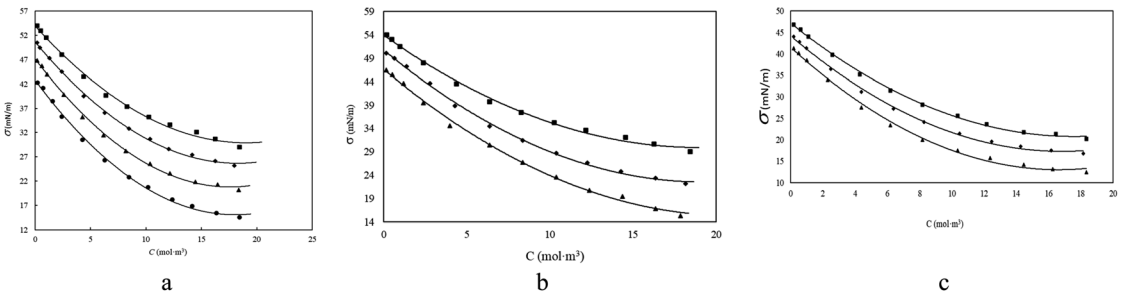

Fig. 2 Surface tension (σ) of SAILs (a) [2-HEA][Lau] in aqueous gabapentin solutions with varying molality concentrations of gabapentin (mol kg^{-1}); ■ 0.0000, ◆ 0.0100 ▲ 0.0300 ● 0.0500 at 298.15 K. (b) ([2-HEA][Lau], [BHEA][Lau] and [T2-HEA][Lau]) in water at 298.15 K: ■, [2-HEA][Lau]; ◆, [BHEA][Lau]; and, ▲, [THEA][Lau]. (c) ([2-HEA][Lau], [BHEA][Lau] and [THEA][Lau]) in aqueous gabapentin solution with 0.03 molality, mol kg^{-1}, concentration at 298.15 K: ■ [2-HEA][Lau], ◆ [BHEA][Lau] and ▲ [THEA][Lau].

In essence, the presence of gabapentin at higher concentrations acts as a trigger for micelle formation at lower SAIL concentrations.

3.2. Surface tension studies

The measured experimental surface tension data for [2-HEA][Lau], [BHEA][Lau], and [THEA][Lau] in various concentrations (0.0000 to 0.0500 mol kg^{-1}) of aqueous gabapentin solution at 298.15 K has been presented in Table S1† through these measurement the interactions between SAILs and various concentrations of gabapentin has been investigated. A meticulous examination of Table 1 revealed a clear inverse correlation between the measured surface tension values and the number of hydroxyethyl groups. This phenomenon aligns with the findings of Pátek and coworkers' study, which investigated the air–liquid interfacial tension of five 1-alkyl-3-methylimidazolium-based ionic liquids with trifluoromethanesulfonate and tetrafluoroborate anions across a temperature range of 268 to 356 K. Utilizing both the Wilhelmy plate and du Noily ring methods, the researchers determined that the Wilhelmy plate method yielded more reliable results with lower standard uncertainty. This study significantly enriched the existing dataset by adding 175 new surface tension measurements to the previously published 50 values for these ionic liquids. A comparison of selected surface tension measurements obtained using the Wilhelmy plate method at 298.15 K demonstrates a consistent decrease in surface tension with increasing alkyl chain length: 1-ethyl-3-methylimidazolium trifluoromethanesulfonate [EMIM][CF_3SO_3] (40.43 mN m^{-1}), 1-butyl-3-methylimidazolium trifluoromethanesulfonate [BMIM][CF_3SO_3] (35.09 mN m^{-1}), and 1-hexyl-3-methylimidazolium trifluoromethanesulfonate [HMIM][CF_3SO_3] (32.37 mN m^{-1}).[25] Additionally the related surface active parameters such as Π (interface surface pressure), σ_{CMC} (CMC point surface tension), A_{min} (minimum surface area occupied per molecule), Γ_{max} (Gibbs maximum excess surface concentration) have been computed through measured surface tension data and has been presented in Table 2 respectively. As it has been illustrated (Fig. 2 and Tables 2, S1†) the surface tension and the CMC point of SAILs show a decreasing trend as the concentration of gabapentin in aqueous solution increases. By utilizing the CMC point values the σ_{CMC} was obtained. The Π, has been used as an illustrator to show the difference between surface tension of the pure solvent and the surface tension of SAILs, and can be calculated through following expression:[26,27]

$$\Pi = \sigma_0 - \sigma \quad (1)$$

Here σ_0, is the surface tension of pure solvent. The Γ_{max}, is a parameter related to describing the surface concentration and it is defined through following formula:[26,27]

$$\Gamma_{max} = -\frac{1}{nRT}\left[\frac{\partial\sigma}{\partial \ln C}\right] \quad (2)$$

where, n is the number of ionic spices resulted of the dissociation of spices in water which in our case is the equivalent of one, R, is the gas constant, T, is the absolute temperature and C, is the concentration of SAILs in the solution. Table 2 presents the Γ_{max} values for the studied SAILs in various concentrations of gabapentin in aqueous solutions. Upon a close inspection it was revealed that as the number of hydroxyethyl groups in the SAILs and concentration of gabapentin drug in aqueous solution increased, the Γ_{max} values exhibited a decreasing trend. This observation in the Γ_{max} values can be attributed to the improved efficiency of the SAILs at the air–water interface. The lower Γ_{max} values in the presence of the various concentration of gabapentin aqueous solution, indicate a decrease in the packing of SAILs molecules at the air/water interface. The A_{min} or the minimum surface area occupied per SAILs molecule can be calculated through the Γ_{max} values which has been expressed as following expression:[26,27]

$$A_{min} = \frac{10^{20}}{N_A \cdot \Gamma_{max}} \quad (3)$$

N_A is the Avogadro number. Also A_{min} illustrates the interface packing of the compactness of the SAILs. The values of A_{min} have been also presented in Table 2, through a careful examination of Table 2, a rising trend for A_{min} values as the number of hydroxyethyl groups, and concentration of the gabapentin in aqueous solution increased was observed. The hydroxyethyl group illustrates greater hydrophilicity features due to their tendency for hydrogen bonding with water molecules. At the interface of water/air, SAILs molecules adsorb with their alkyl chains oriented toward the air, which would cause them to have minimum contact with the aqueous phase. As the number of hydroxyethyl groups increases a more prominent hydrophobic effect drives the SAILs to the interface, leading to denser packing and lower surface tension. The alkyl chain, prefers to minimize its contact with water. Introducing additional hydroxyethyl groups, with their hydrophilic nature, introduces steric hindrance at the interface. This steric effect necessitates a larger minimum surface area to accommodate the SAIL molecule. Consequently, less energy is required to create a new surface area, resulting in a decrease in the Γ_{max}. Conversely, as the number of hydroxyethyl groups increases, the hydrophilicity of the SAILs weakens, hindering their ability to pack at the interface effectively. The introduction of gabapentin molecules in the aqueous solution further influences the surface activity of SAILs. At higher concentrations, gabapentin may compete with the SAILs for favorable positions at the interface, disrupting their packing efficiency and potentially increasing the minimum area occupied per molecule. This disruption could explain the observed decrease in excess surface concentration with increasing gabapentin concentration.

Tables 2 and S6, S7† presents the thermodynamic parameters of micellization expressed by standard free energy of micellization ΔG_{mic}, enthalpy of micellization ΔH_{mic}, free energy of surface at equilibrium G^s_{min}, and standard Gibbs free energy of adsorption ΔG^0_{ad}, for the investigated SAILs are calculated from the following equations:[28]

$$\Delta G_{mic} = RT \ln X_{cmc} \quad (4)$$

$$\Delta H_{mic} = \Delta G_{mic} + T\Delta S_{mic} \quad (5)$$

$$-\Delta S_{mic} = \left(\frac{\partial \Delta G_{mic}}{\partial T}\right) \quad (6)$$

$$G^s_{min} = A_{min} \cdot \gamma_{CMC} \cdot N_A \quad (7)$$

$$\Delta G^0_{ad} = \Delta G^0_{mic} - \frac{\pi_{CMC}}{\Gamma_{max}} \quad (8)$$

In the above-cited expressions, X_{cmc} illustrates the mole fractional concentration of the employed additives. Table 2 depict the evaluated ΔG_{mic}, G^s_{min}, and ΔG^0_{ad}, and Tables S6 and S7† represents the values of ΔH_{mic} for the current studied systems. Analyzing the thermodynamic parameters of micellization from Tables 2 and S6, S7,† it may conclude that micellization process is spontaneous, ΔG_{mic} values for studied SAILs are negative ($\Delta G_{mic} < 0$) and these values become more negative in presence of gabapentin. Among the laurate SAILs ([THEA][Lau], [BHEA][Lau], and [2-HEA][Lau]), ΔG_{mic} values were found to become less negative with the decrease in number of hydroxyethyl groups (from three to mono). Such a decrease in ΔG_{mic}, with an increase in the number of hydroxyethyl group, could be related to more hydrogen bonding upon micellization. Through a comparison of the ΔG^0_{ad}, and ΔG_{mic} presented in Table 2 for the studied SAILs, it was revealed that the values of Gibbs free energy of adsorption are more negative than Gibbs free energy of micellization, which suggest that the adsorption process can be the primary process. This observation signifies that, from a thermodynamic standpoint, adsorption can be the preferred process for these SAILs.[29–31] Also, from a close inspection of the manuscript, we realize that the values of ΔG^0_{ad} for [THEA]Lau with higher number of hydroxyethyl groups are more negative in comparison to [2-HEA]Lau with lesser number of hydroxyethyl groups which ultimately could indicate that [THEA]Lau is the most suitable candidate in increasing the adsorption of gabapentin in the gastrointestinal region among other SAILs studied.

Interestingly Table 2 present positive values for G^s_{min}, (free energy of the surface at equilibrium), this doesn't contradict the preferential adsorption observed. G^s_{min} reflects the energy required to create a unit area of the new surface with adsorbed SAIL molecules. The positive value indicates that some energy input is necessary to form this new surface. However, the overall adsorption process remains thermodynamically favorable because the values of G^s_{min} are small despite being positive and decrease in ΔG^0_{ad} (more negative value) outweighs the increase in G^s_{min}. Essentially, the energy gained from the favorable

interaction between the SAILs and the surface outweighs the energy cost associated with creating the new surface.[29–31]

3.3. Electrical conductivity studies

Tables S8–S11† illustrates the related values of molar conductivity, Λ, for studied SAILs of [2-HEA][Lau], [BHEA][Lau] and [THEA][Lau] in water at varying temperature and in aqueous gabapentin solutions at 298.15 K. The molar conductivity, Λ, have been computed in order to investigate the interactions between gabapentin and SAIL in aqueous media. In Fig. S7,† these values are also shown graphically *versus* the concentration of SAILs at different molalities of gabapentin. The molar conductivities clearly decrease as the concentrations of SAILs increases. These values also decrease with an increase in the content of gabapentin drug. The following equations were used to evaluate the experimental data using the low concentration Chemical Model (lcCM):[2,32–34]

$$\Lambda = \alpha[\Lambda_0 - S(c\alpha)^{1/2} + Ec\alpha \ln(c\alpha) + J_1 c\alpha + J_2(c\alpha)^{3/2}] \quad (9)$$

$$K_A = \frac{1-\alpha}{\alpha^2 c \gamma_{\pm}^2} \quad (10)$$

$$\ln \gamma_{\pm} = -\frac{kq}{1+kR} \quad (11)$$

$$k^2 = \frac{16000 N_A z^2 e^2 \alpha c}{\varepsilon_0 \varepsilon k_B T} \quad (12)$$

$$q = \frac{z^2 e^2}{8\pi\varepsilon_0 \varepsilon k_B T} \quad (13)$$

Here Λ is the molar conductivity and Λ_0 is the limiting molar conductivity, $(1-\alpha)$ is the percentage of oppositely charged ions functioning as ion pairs, R is a distance parameter, and $\gamma_{\pm}$ is the corresponding mean activity gabapentin of free ions. The numbers needed for the coefficients E, J_1 and J_2 computations were obtained from Barthel and co-workers.[32] In this equation, c is the molar concentration of SAILs computed from the solution's molality and density values. The remaining parameters have their normal meanings. Non-linear least-squares iteration on the molar conductivity data yields the K_A, the Λ_0, and R. Tables 3 and S12,† displays the values of K_A, Λ_0, and R for binary and ternary systems. In these Tables, the values of Λ_0 and K_A decrease and increase as gabapentin concentration increases. This occurrence can be explained by the fact that as gabapentin concentration increases, (i) the interactions of SAILs and gabapentin become stronger, resulting in an increase in the radii of solvated ions and thus mobility, and (ii) the mobility of ions decreases due to an increase in the viscosity of the solution. Also, the values of Λ_0 in all studied systems decrease as number of hydroxyethyl group of SAILs increases due to a decrease in mobility of SAILs.

3.4. Theoretical framework

The theoretical framework of the study has been primarily set upon the DFT calculation on Dmol3 with COSMO results. Materials Studio (Biovia, 2023) employing the GGA VWN-BP functional was used to achieve the optimal results for the studied system, as recommended by the Dmol3 developers. Also, water was chosen as the solvent for the COSMO calculation. A two-step task including geometry and energy optimization GGA VWN-BP function, DND (3.5) basis set, and COSMO results. Fig. 3 depicts the COSMO results containing σ-profile and the optimized molecular structures of the studied materials. A hallmark of COSMO-based thermodynamics is the σ-profile, a molecular fingerprint that characterizes the surface

Table 3 The association constants (K_A), limiting molar conductivities (Λ_0), the distance of closest approach of ions (R), and standard deviations ($\sigma(\Lambda)$) of EALau in ternary aqueous[a] solutions at 298.15 K

m (mol kg^{-1})	K_A (dm^3 mol^{-1})	Λ_0 (S cm^2 mol^{-1})	$10^{10}R$ (mol kg^{-1})	($\sigma(\Lambda)$)
[2-HEA][Lau] in aqueous solution of gabapentin				
0.0000	550	70	7	1.1
0.0098	0.138	48.881	59.65	0.32
0.0303	525.631	47.777	10.57	0.18
0.0497	139.179	31.736	46.21	0.05
[BHEA][Lau] in aqueous solution of gabapentin				
0.0000	1512	66.819	8	0.92
0.0103	1338	48.432	50	0.84
0.0303	2462	45.913	50	1.19
0.0496	1000	30.676	40	0.7
[THEA][Lau] in aqueous solution of gabapentin				
0.0000	3629.00	49.932	50	1.29
0.0103	3715.00	45.77	50	1.14
0.0304	927.065	21.155	10	1.11
0.0505	1254.000	20.00	0.1	1.24

[a] The standard uncertainties for molality and temperature were $u(C) = 0.001$ mol m^{-3} and $u(T) = 0.5$ K, respectively with level of confidence 0.95. The standard combined uncertainty for conductance and molar conductivity were about, $uc(\kappa) = 0.5$ μS cm^{-1} and $uc(\Lambda) = 0.7$ S m^2 mol^{-1} (level of confidence 0.68), respectively.

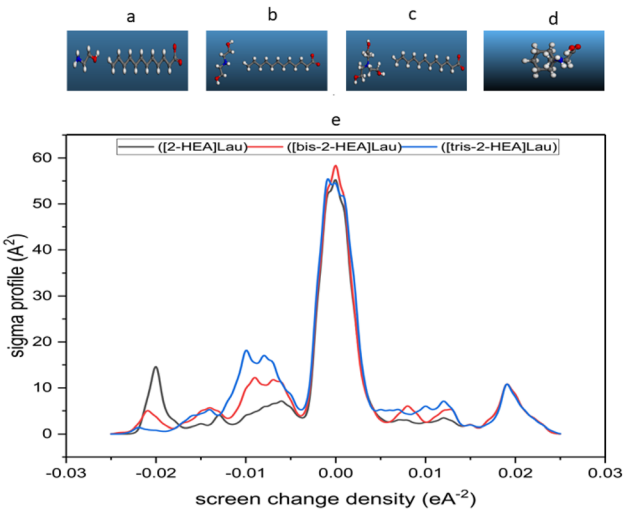

Fig. 3 Optimized molecular structure and σ-profile of (a) [2-HEA][Lau], (b) [BHEA][Lau], (c) [THEA][Lau], (d) gabapentin and (e) sigma profile plot from Dmol3 and COSMO result.

Table 4 The surface area and total volume of cavity, dielectric (solvation) energy, HOMO and LUMO values obtained from COSMO and Dmol3 calculations

Material	A (A^2)	V (A^3)	Dielectric (solvation) energy (kcal mol^{-1})	HOMO	LUMO
Gabapentin	198.232418	202.454296	−26.60	47	48
[2-HEA][Lau]	384.909679	349.45272	−136.93	73	74
[BHEA][Lau]	432.935659	411.490573	−128.79	85	86
[THEA][Lau]	477.104013	453.628474	−127.03	97	98

charge distribution.[35,36] This profile provides valuable insights into the probability of specific charge concentrations within defined molecular segments. COSMO models, such as COSMO-RS and COSMO-SAC, utilize σ-profiles to predict thermodynamic properties and interactions with the environment.

Typically, σ-profiles are derived from computationally intensive simulations of molecular electron density using density functional theory (DFT). This computational bottleneck often limits the widespread application of theoretical approaches. The σ-profile serves as a powerful tool for analyzing the electronic charge distribution on molecules. It offers valuable insights into molecular polarity, reactivity, and intermolecular interactions.[37,38] In the context of ionic liquids, σ-profiles aid in understanding the charge distribution between the cation and anion, a crucial factor in determining their unique properties.[39,40]

By examining a molecule's σ-profile, one can identify regions of high and low electron density. These regions correlate with the presence of functional groups, such as polar groups or aromatic rings, which influence molecular reactivity and properties. Moreover, σ-profiles can be used to predict a molecule's dipole moment and its interactions with other molecules, including solvents and charged species. The Fig. 3 depicts the σ-profile density distributions of four surface active ionic liquids (SAILs) and gabapentin, as derived from COSMO analysis using Dmol3. The predominant negative charge density observed in most distributions is a characteristic feature of ionic liquids due to the significant charge separation between the cation and anion. The peaks in the σ-profiles correspond to regions of highest electron density. For SAILs, these peaks are located around sigma values of −0.02 to 0.02, indicating a relatively broad distribution of negative charge across the molecular surface. In contrast, gabapentin's peak is narrower and centered around −0.01, suggesting a more localized negative charge distribution.

The height of these peaks reflects the magnitude of the negative charge density. SAILs with longer alkyl chains ([BHEA][Lau] and [THEA][Lau]) exhibit higher peaks than the shorter chain SAIL ([2-HEA][Lau]), indicating a greater concentration of negative charge on the longer chains. The negative charge distribution in SAILs and gabapentin can be attributed to the presence of charged head groups. Oxygen atoms within these head groups tend to have a higher electron density than carbon atoms in the alkyl chains, resulting in a negative charge concentration in the head group region. The broader peak observed for longer chain SAILs suggests a more delocalized negative charge along the alkyl chain, possibly due to increased chain flexibility. In contrast, gabapentin's narrower peak indicates a more localized negative charge distribution, potentially influenced by the presence of the aromatic ring and hydroxyl group. The negative charge distribution in SAILs and gabapentin has implications for their properties and interactions with other molecules. For instance, the presence of a negative charge can enhance interactions with positively charged surfaces or molecules, such as proteins or nanoparticles. Additionally, the negative charge can influence the solubility of SAILs in water and other polar solvents.

Also, the related dielectric (solvation) energy and other properties that could be used for interpretation of hydration behavior of the SAILs and the drug besides the cavity surface area and volume that has presented in Table 4. The related values for solvation energy gets slightly positive with an increase in the number of hydroxyethyl group from [2-HEA] to [THEA] (*e.g.* solvation energy for [2-HEA][Lau] is −136.93 kcal mol^{-1} while for [THEA][Lau] is −127.03 kcal mol^{-1}). The observed increase in surface area (A) and volume of the cavity (V) as the number of hydroxyethyl groups increase can be attributed to the structural changes in the molecules. Additional hydroxyethyl groups lead to a more extended and complex molecular structure, resulting in a larger surface area and volume of the cavity. This increase in size allows for more interactions with the surrounding solvent molecules, potentially enhancing the solvation process. The slight increase in solvation energy with an increase in the number of hydroxyethyl groups from [2-HEA] to [THEA], could be due to the introduction of additional functional groups that alter the solute–solvent interactions. The presence of more hydroxyethyl groups may disrupt the existing solute–solvent interactions or introduce steric hindrance, leading to a less favorable solvation energy.[35,41]

4. Conclusion

In this study, the electrical conductivity and surface tension measurement has been utilized in order to determine the CMC of some SAILs [2-HEA][Lau], [BHEA][Lau], and [THEA][Lau] in aqueous media at different temperatures and at various concentrations of gabapentin drug in aqueous solutions. The results indicate the CMC values were increased with the temperature increasing up to 303.15 K and then decrease. Accordingly; the thermodynamic properties of the CMC have been calculated based on the equilibrium constant by Gibbs free energy of micellization. It was observed that, in presence of

gabapentin drug was decrease CMC point of the SAILs which is due to strong interactions between the drug and SAILs. Finally, the interaction of mentioned SAILs and gabapentin with calculation of limiting molar conductivity, Λ_0, and associated constant, K_A, has been investigated. The results show that, the interactions between SAILs and drug were increased with increasing the drug concentration.

COSMO and Dmol3 results were utilized to study the effect of structure of molecules on their interactions with water solvent. It was found that molecules with more hydroxyethyl groups have a larger surface area and cavity volume. The larger size allows for more contact with the solvent molecules, leading to better solvation. A more negative solvation energy indicates a stronger and more favorable interaction between the molecule and the solvent. Finally, the study observed that both HOMO and LUMO energy levels increase with more hydroxyethyl groups. This is due to the increased number of electrons and energy levels in larger molecules. Higher HOMO levels suggest more stability, while higher LUMO levels indicate a wider range of possible electronic transitions for the molecule.

Data availability

The authors confirm that the data supporting the findings of this study are available within the manuscript, figures, tables, and ESI† files.

Conflicts of interest

The authors declare that they have no known competing financial interests or personal relationships that could have appeared to influence the work reported in this paper.

Acknowledgements

The authors wish to thank financial support from the graduate council of the University of Tabriz, Tabriz, Iran.

References

1 S. K. Nandwani, N. I. Malek, M. Chakraborty and S. Gupta, *Energy Fuels*, 2020, **34**, 6544–6557.
2 M. Bagheri, H. Shekaari, F. Ghaffari and F. Mousavi, *J. Mol. Liq.*, 2024, **397**, 124125.
3 A. Zendehbad, M. Bagheri, M. Mokhtarpour, H. Shekaari and M. T. Zafarani-Moattar, *J. Chem. Eng. Data.*, 2024, **69**(7), 2528–2545.
4 H. Kandar, S. K. Das, L. Ghosh and B. K. Gupta, *J. PharmaSciTech*, 2012, **1**, 20–26.
5 C. E. Stafstrom, *J. Cereb. Blood Flow Metab. Suppl.*, 2006, **26**, 983–1004.
6 H. Rayner, J. Baharani, S. Smith, V. Suresh and I. Dasgupta, *Nephron Clin. Pract.*, 2013, **122**, 75–79.
7 J. Slater, S. Chung, L. Huynh, M. S. Duh, B. Gorin, C. McMicken, A. Ziemann and J. Isojarvi, *Epilepsy Res.*, 2018, **143**, 120–129.
8 O. E. Veronica and A. M. Emmanuella, *Afr. J. Educ. Sci. Technol.*, 2017, **3**, 59–62.
9 S. S. Kwon, B. J. Kong, W. G. Cho and S. N. Park, *Korean J. Chem. Eng.*, 2015, **32**, 540–546.
10 K.-S. Kim, D. Demberelnyamba, B.-K. Shin, S.-H. Yeon, S. Choi, J.-H. Cha, H. Lee, C.-S. Lee and J.-J. Shim, *Korean J. Chem. Eng.*, 2006, **23**, 113–116.
11 V. N. Patil, M. Basu, P. A. Hassan, B. Dutta, V. Patil and S. S. Bhawal, *J. Mol. Liq.*, 2024, **411**, 125733.
12 S. Chen, X. Zhou, J. Yang, Y. Dai, W. Wang, W. Jiang, X. Li and J. Zhang, *J. Mol. Liq.*, 2023, **390**, 123072.
13 A. Javadi, S. Dowlati, S. Shourni, R. Miller, M. Kraume, K. Kopka and K. Eckert, *Adv. Colloid Interface Sci.*, 2022, **301**, 102601.
14 M. Bagheri, H. Shekaari, M. Mokhtarpour, F. Ghaffari, S. Faraji and B. Golmohammadi, *J. Chem. Eng. Data*, 2023, **69**, 114–127.
15 J. Liu, D. Jiang, H. Fei, Y. Xu, Z. Zeng and W. Ye, *Mater. Today Commun.*, 2022, **31**, 103325.
16 J. Dai, F. Ma, Z. Fu, C. Li, M. Jia, K. Shi, Y. Wen and W. Wang, *Renewable Energy*, 2021, **175**, 748–759.
17 W. Xu, Q. Zhang, H. Wei, J. Qin and L. Yu, *J. Surfactants Deterg.*, 2015, **18**, 421–428.
18 J. Jiao, B. Han, M. Lin, N. Cheng, L. Yu and M. Liu, *J. Colloid Interface Sci.*, 2013, **412**, 24–30.
19 G. Stirnemann, F. Sterpone and D. Laage, *J. Phys. Chem. B*, 2011, **115**, 3254–3262.
20 A. Banerjee and B. Das, *Z. Phys. Chem.*, 2024, **238**, 571–591.
21 S. Ahsan, A. Dhanagar and A. Shaheen, *Tenside Surfactants Deterg.*, 2023, **60**, 356–367.
22 D. Ray, S. Das, R. De and B. Das, *Carbohydr. Polym.*, 2015, **125**, 255–264.
23 G. Singh, G. Singh and T. S. Kang, *Phys. Chem. Chem. Phys.*, 2018, **20**, 18528–18538.
24 M. Bagheri, H. Shekaari, M. Mokhtarpour, F. Ghaffari, S. Faraji and B. Golmohammadi, *J. Mol. Liq.*, 2024, **397**, 124063.
25 M. Součková, J. Klomfar and J. Pátek, *Fluid Phase Equilib.*, 2011, **303**, 184–190.
26 A. Shaheen, R. Arif and S. Rehman, *Colloid Interface Sci. Commun.*, 2019, **33**, 100204.
27 B. N. Tackie-Otoo, M. A. Ayoub Mohammed, H. A. B. M. Zalghani, A. M. Hassan, P. I. Murungi and G. A. Tabaaza, *Molecules*, 2022, **27**, 2265.
28 Z. H. Asadov, R. A. Rahimov, S. M. Nasibova and G. A. Ahmadova, *J. Surfactants Deterg.*, 2010, **13**, 459–464.
29 C. Bermúdez-Salguero and J. Gracia-Fadrique, *J. Colloid Interface Sci.*, 2011, **355**, 518–519.
30 R. Kamboj, P. Bharmoria, V. Chauhan, G. Singh, A. Kumar, S. Singh and T. S. Kang, *Phys. Chem. Chem. Phys.*, 2014, **16**, 26040–26050.
31 A. A. Thoppil, B. K. Chennuri and R. L. Gardas, *J. Mol. Liq.*, 2020, **299**, 112116.
32 J. M. G. Barthel, H. Krienke and W. Kunz, *Physical Chemistry of Electrolyte Solutions: Modern Aspects*, Springer Science & Business Media, 1998, vol. 5.

33 A. Mehrdad, H. Shekaari and N. Noorani, *J. Mol. Liq.*, 2018, **255**, 454–461.
34 H. Shekaari, M. T. Zafarani-Moattar and S. Faraji, *J. Chem. Eng. Data*, 2021, **66**, 1890–1899.
35 M. A. Morsali, B. Golmohammadi and H. Shekaari, *Sci. Rep.*, 2024, **14**, 20372.
36 S. Gharehzadeh Shirazi, S. Shahabadi, H. Shekaari and B. Golmohammadi, *J. Chem. Eng. Data*, 2023, **68**, 3126–3134.
37 M. R. Islam and C.-C. Chen, *Ind. Eng. Chem. Res.*, 2015, **54**, 4441–4454.
38 D. O. Abranches, E. J. Maginn and Y. J. Colón, *J. Chem. Theory Comput.*, 2023, **19**, 9318–9328.
39 Y.-R. Tsai and S.-T. Lin, *Ind. Eng. Chem. Res.*, 2019, **58**, 10064–10072.
40 D. Moreno, M. Gonzalez-Miquel, V. R. Ferro and J. Palomar, *ChemPhysChem*, 2018, **19**, 801–815.
41 L. Del Olmo, I. Lage-Estebanez, R. López and J. M. García De La Vega, *J. Phys. Chem. B*, 2016, **120**, 10327–10335.